Efficient Temporal Compression of Coherent Nanosecond Pulses in a Compact SBS Generator-Amplifier Setup

Stephan Schiemann, Wim Ubachs and Wim Hogervorst

Abstract— A pulse compressor based on stimulated Brillouin scattering (SBS) in liquids is experimentally and theoretically investigated. It allows for the compression of Fourier-transform limited nanosecond pulses of several hundreds of millijoules of energy with both high conversion efficiency and a high temporal compression factor. The two-cell generator-amplifier arrangement is of a compact design not requiring external attenuation of the generator cell input energy. Pulses from an injection-seeded, frequency-doubled Nd:YAG laser of 300-mJ energy were compressed by a factor variable between 6 and 21 at up to 75% reflectivity. Deviation from unity SBS reflectivity is predominantly determined by optical component losses. The generation of 270-ps pulses with high beam quality was achieved in liquid methanol. These powerful pulses of variable duration are difficult to produce with common laser systems and are highly suited for the generation of high-harmonics in gases.

Index Terms— Brillouin scattering, Nd:YAG lasers, optical pulse compression, pulse compression methods, pulsed lasers.

I. INTRODUCTION

THE phenomenon of stimulated Brillouin scattering (SBS) in liquid or gaseous media, discovered some 30 years ago [1], is nowadays widely employed to realize phase-conjugating mirrors [2]. It can be used as well to temporally compress nanosecond pulses [3]. The design of SBS-based compressors for the generation of subnanosecond pulses at energies approaching the Joule level is an active field of research [4], [5]. They offer the prospect of achieving a conversion efficiency of nearly unity, thus providing enhancement of peak intensity of a pulse while maintaining its high energy. These compressors also make available laser pulses in the time window 300–3000 ps, which is difficult to access by mode-locking or Q-switching techniques.

High-energy SBS compressors presented in literature often do not achieve high efficiencies due to multimode radiation input [6], [7] or they involve complex optical designs of combined SBS cells and laser amplifier stages [5], [4], [6]. In this paper, we present an effective and compact SBS compressor to manipulate Fourier-transform limited pulses of nanosecond duration. In the setup *simultaneously* a high conversion efficiency of 90%, only limited by reflection losses,
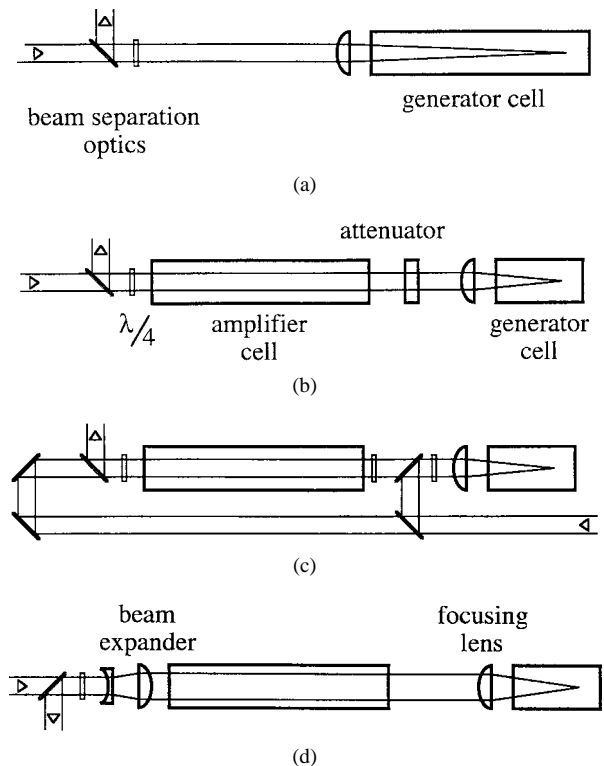
Fig. 1. Various high-energy SBS compressor concepts: (a) single-cell generator with long focal-length lens, (b) two-cell generator-amplifier setup with attenuator in front of generator cell, (c) two-cell generator-amplifier setup with generator cell separately pumped by a small fraction of pump pulse energy, and (d) compact SBS generator-amplifier setup, presented in this study.

and a compression factor of up to 21 is obtained in liquid Brillouin-active media for input energies of several 100 mJ of visible light. The setup contains only a few optical elements and permits easy adjustment of the pulse duration between 300 and 3000 ps.

II. THE COMPACT SBS GENERATOR-AMPLIFIER SETUP: THEORY

A. Concept

For both SBS phase-conjugating mirrors and SBS pulse compressors, two general types of cell-arrangements exist [5], [8]: the single-cell SBS generator (or tapered waveguide [9]) and the multiple-cell SBS generator-amplifier setup. These types are schematically depicted in Fig. 1. The single-cell

generator [Fig. 1(a)] is not suitable to efficiently compress high-energy pulses because it provides high conversion efficiency only at low input energy [9], [10] ,[7]. At high input energy, a poor efficiency [4] or only a weak compression was achieved [3]. A two-cell generator-amplifier arrangement can overcome these limitations. In Figs. 1(b)–(d), different realizations are shown, which are suitable for high-energy compression [11], [6], [5], [9]. As a protection against too-high peak intensities being launched into the generator cell, either an attenuator is introduced [Fig. 1(b)] or the pump beam is split up into a weak part, pumping the generator cell, and a strong part passing the amplifier cell [Fig. 1(c)]. In the following, we will present and discuss the scheme illustrated in Fig. 1(d), which we will refer to as the "compact SBS generator-amplifier setup" (CGAS). In this arrangement, no optical components are mounted that limit the generator cell input. The concept of this compressor was described before [9], [8], however, without addressing its potential to achieve subnanosecond output at high conversion efficiency.

The functional concept of the CGAS may be described as follows: a short focal-length lens in front of the generator is introduced to create stimulated Brillouin radiation from the leading edge of the pump pulse. The back-scattered beam seeds the amplifier located at minimum distance of the generator cell. The sustained interaction of pump and Stokes radiation in the amplifier cell automatically controls and limits the generator-cell input energy. In addition, the SBS pulse experiences strong intensity amplification and a substantial temporal reshaping in the amplifier cell. As a result, the Stokes pulse duration drops below the acoustic phonon lifetime in the SBS medium and the CGAS approaches a reflectivity of nearly 100%. These effects will be discussed in detail in the following section. The concept of automatic attenuation of the generator-cell input energy, inherent to the CGAS, was already investigated before [12]–[14], but these studies solely concentrated on steady-state pump depletion and did not pursue temporal pulse shaping, as is the subject of the present study.

To achieve a high conversion efficiency in the compressor, it is crucial to apply nearly Fourier-transform-limited input pulses. The absence of short-lived intensity spikes in the temporal domain in these pulses effectively prevents the generation of stimulated Raman scattering, a process strongly competitive to SBS [15], [16], [4]. Liquids are favored over gases as Brillouin-active media. To achieve adequate SBS gain in gases and to compete against stimulated Raman scattering, high gas pressures of 10–100 bar would be necessary [17], [18]. Apparently the need for high-pressure cells would then contradict a simple compressor design.

B. Numerical Model

In this paragraph, a numerical model of the compact SBS generator-amplifier setup (CGAS) is introduced. It allows a simple way to analyze the process of pulse compression in the CGAS in order to ascertain its optimum operation conditions.

1) Coupled Equations Describing SBS: Stimulated Brillouin Scattering is a three-wave parametric mixing process coupling two radiation fields (the incident pump field $\tilde{E}_p$ and the created Stokes field $\tilde{E}_s$) with an acoustic matter-density field $\tilde{\rho}$ in the active medium. The fields will be described as plane waves propagating along the z axis:

$$\tilde{E}_p(z,t) = \tfrac{1}{2}\ E_p(z,t)e^{i(k_p z - \omega_p t)}ad\ +\ c.c.$$
$$\tilde{E}_s(z,t) = \tfrac{1}{2}\ E_s(z,t)e^{i(-k_s z - \omega_s t)}\ +\ c.c.$$
$$\tilde{\rho}(z,t) = \tfrac{1}{2}\ \rho(z,t)e^{i(k_B z - \omega_B t)}\ +\ c.c. \qquad (1)$$

with $\omega_B = \omega_p - \omega_s$ and $k_B = k_p - k_s$. The polarization state of the radiation is neglected, because SBS represents a polarized scattering process [19]. The application of a one-dimensional (1-D) model assumes that the spatial profile of the laser beam has a constant intensity. A two-dimensional (2-D) calculation, which could take into account realistic nonuniform beam profiles of pulsed sources, is impeded since it would require excessive computational time.

The propagation of the acoustic phonon wave is modeled by introducing well-established approximations. In a nonabsorbing medium, phonons are created only by electrostrictive coupling under adiabatic conditions, and their amplitudes are small enough to allow linearization of the equations. The wave-equation is derived from the acoustic Euler equation, including a simple damping term and the electrostrictive force [19]:

$$\frac{\partial \rho}{\partial t} + \tfrac{1}{2}\Gamma_B \rho = \frac{i}{16\pi}\frac{\gamma_e k_B^2}{\omega_B}E_p E_s^* \qquad (2)$$

Here, $\Gamma_B = k_B^2 \Gamma'$ represents the phonon relaxation rate, Γ' the damping parameter [19], and γ_e the electrostrictive coupling constant. By assuming the pump laser pulse duration τ_p to be large compared to the phonon lifetime τ_B, it is valid to apply the slowly varying amplitude approximation and to omit second-order time-derivatives $\partial^2/\partial t^2$. In addition, the spatial derivative $\partial/\partial z$ can be neglected for short phonon lifetimes.

The propagation of pump and Stokes waves under phase-matching conditions can be modeled straightforwardly [20]:

$$\frac{n}{c}\frac{\partial E_p}{\partial t} + \frac{\partial E_p}{\partial z} = i\frac{\omega_p \gamma_e}{4nc\rho_0}\rho E_s$$
$$\frac{n}{c}\frac{\partial E_s}{\partial t} - \frac{\partial E_s}{\partial z} = i\frac{\omega_s \gamma_e}{4nc\rho_0}\rho^* E_p \qquad (3)$$

with ρ_0 the average density and n the refractive index of the medium.

2) Numerical Solution of the Coupled Equations: After choosing proper initial conditions the complex equations (2) and (3) transform to a set of equations with real variables $E_p' = Re(E_p)$, $E_s' = Im(E_s)$, $\rho' = Re(\rho)$ and g_1, g_2 representing the photon-phonon coupling constants in (3) and (2), respectively:

$$g_1 = \frac{\gamma_e \omega_p}{4nc\rho_0} \quad g_2 = \frac{\gamma_e k_B^2}{16\pi\,\omega_B}. \qquad (4)$$

The fact that pump and Stokes fields are counterpropagating needs special consideration when selecting an algorithm for the numerical solution of the coupled equations. It is realized by transforming (3) along their characteristics, hence integrating on a space-time grid (z_i, t_j) of stepsize $\Delta z = \pm c/n\,\Delta t$. The resulting new set of equations involves only time-derivatives
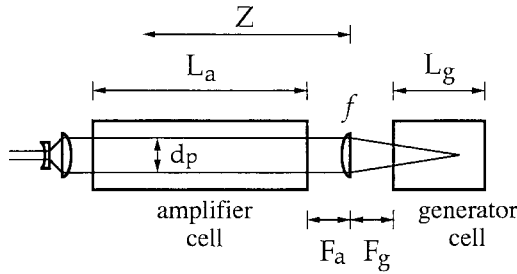
Fig. 2. Dimensions of the compact SBS generator-amplifier setup. The beam diameter d_p is controlled by beam-expansion optics in front of the amplifier. In the numerical model, $F_a = F_g = 0$; in the experiment, $F_a = F_g \approx 0.5$ cm is chosen.

TABLE I
COMPILATION OF PARAMETERS CHARACTERIZING THE
SBS LIQUIDS: STEADY-STATE SBS GAIN g_B AND
ACOUSTIC PHONON LIFETIME τ_B AT $\lambda_p = 532$ nm

	g_B [20] [cm/MW]	g_B [22] [cm/MW]	τ_B [20] [ps]	τ_B [22] [ps]	ω_B [20] [10^{10} s^{-1}]	$\bar{\rho}/\rho_0$
Water	0.0048	0.0038	295	471	4.664	10^{-8}
Methanol	0.0130	---	374		3.484	10^{-9}
CCl$_4$	0.0060	0.0038	144	151	3.598	—

Acoustic phonon frequency ω_B at $\lambda_p = 532$ nm and thermal acoustic condensation $\bar{\rho}/\rho_0$ (derived numerically). All data from [20] and [22]

and is solved to a self-consistent solution by iteration. Because pulse rise times of less than 100 ps and extreme field strength variations, especially in the generator cell, have to be considered, the value of the integration time step Δt was controlled by the program, between 0.2 ps and 0.004 ps. A simulation took 8 h of CPU time on a PPC 604 (100 MHz).

Focusing in the active medium is simulated by a stepwise correction of the pump and Stokes amplitudes E_p', E_s' during the integration along the z-axis according to the decreasing beam diameter behind the lens. To initiate the conversion of pump into Stokes radiation, controlled by (3), a constant level of phonon amplitude $\bar{\rho}$ is introduced as an initial condition on grid points inside the SBS cells. It simulates thermal phonon population being the source of spontaneous Brillouin scattering [21].

3) Input Parameters and their Accuracy: In the model for the CGAS, we used the following experimental values: $L_a = 1$ m, $L_g = 0.3$ m, $F_a = F_g = 0$ ($F_a = F_g \approx 0.5$ cm in the experiments), $f = 10$ cm. These parameters are defined in Fig. 2. Pump pulses for a Gaussian temporal profile of duration $\tau_p = 5.6$ ns (FWHM of intensity) are considered. For a given pulse energy, the electric peak field strength is derived by assuming a circular spatial beam profile of constant intensity and of diameter $d_p = 6.5$ mm. The parameter τ_s defines the duration of the back-scattered Stokes pulse.

The parameters g_B, τ_B, and ω_B to characterize the applied SBS liquids water, methanol, and CCl$_4$, respectively, were derived from data in [22] and [20], i.e., they were corrected to $\lambda_p = 532$ nm by means of their specific dependence on the input wavelength [19]. The results are listed in Table I. Preference was given to g_B values from [20], because they agreed best with our experimental observations.

A characteristic problem of published values for τ_B is that phonon lifetimes of SBS liquids are usually not measured directly in the time domain but are derived from Brillouin frequency linewidth data [22], [23]. This may give rise to an inherent source of confusion as these measurements can be performed either in a spontaneous or stimulated scattering process [20]. In addition, experimentally determined Brillouin lineshape profiles presented in the literature vary between Lorentzian and Gaussian or even more complicated structures [24], [23]. As a consequence, there exists no unique way of extracting values for τ_B from these data and, consequently, published phonon lifetime values possess a rather high uncertainty.

The value g_B is defined for monochromatic excitation under steady-state conditions [19], therefore, in our model at pulsed excitation it holds as an upper limit to determine g_1 and g_2 in (3) and (2) by the relation

$$g_B = \frac{\gamma_e^2 \omega_p^2}{n v c^3 \rho_0 \Gamma_B} = g_1 g_2 \frac{n}{c} \frac{32\pi}{\Gamma_B} \qquad (5)$$

if the approximations $k_B = 2k_p$ and $\omega_B = 2nv\omega_p c^{-1}$ are applied. The parameter v, which represents the velocity of hypersound in the SBS medium, and all remaining parameters were taken from [25].

The parameter $\bar{\rho}$, which represents the thermal phonon amplitude, is empirically derived in our model: simulating an unfocused pump beam of high energy entering a single amplifier cell, the level $\bar{\rho}$ for each SBS liquid is adjusted in such a way that the resulting SBS reflectivity of the amplifier cell fits the experimentally observed value. The values are listed in Table I.

C. Numerical Results for Compressing High-Energy Pulses

Due to the low accuracy of several of the input parameters, it is not useful to simply reproduce experimental data numerically. Instead we will concentrate on using the model to generate data which are essential to understand the CGAS principle and usually difficult to extract from the experiments. The term conversion efficiency or reflectivity of the CGAS defines the percentage of emitted Stokes pulse energy related to the input pump pulse energy. The term compression factor defines the ratio between time durations of the primary Stokes pulse and the pump pulse.

First a single-cell SBS generator ($L_a = 0$, $L_g = 1$ m, $f = 95$ cm) is simulated to demonstrate its limitations at high-energy input. Results are shown in Fig. 3. Water possesses a relatively large phonon lifetime and is chosen as the SBS medium for ease of graphical presentation of the emission structures. Above the SBS threshold, both the reflectivity and compression factor rise with increasing input energy. At 10-mJ input, a compression factor corresponding to $\tau_s \approx \tau_B$ is achieved at 89% reflectivity. Larger energies cause complications: after the primary Stokes pulse has left the cell, the remaining part of the pump pulse—still highly energetic—generates secondary Stokes emission. This secondary emission is characterized by strong "ringing structures" caused by SBS back-conversion of Stokes into pump radiation and vice versa [17]. It results
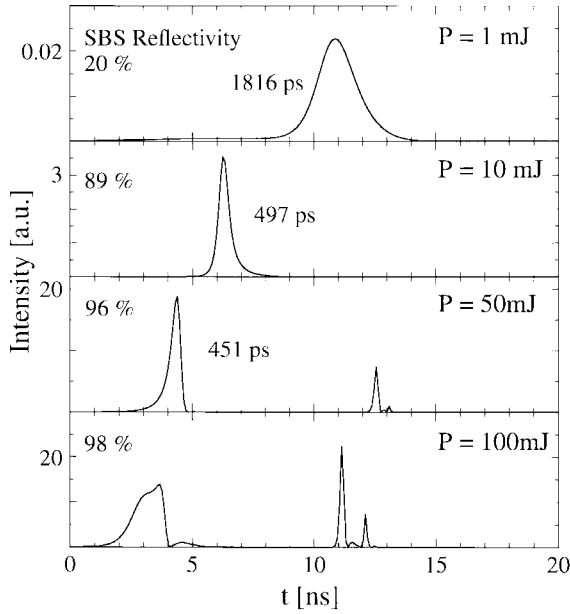
Fig. 3. Numerically generated temporal intensity profiles of SBS pulses emitted from a single-cell SBS generator (water, $f = 95$ cm), plotted at various input energy levels P. Input parameters are $L_a = 0$, $L_g = 95$ cm, $F_a = F_g = 0$, $d_p = 6.5$ mm as defined in Fig. 2 and $\lambda_p = 532$ nm, $\tau_p = 5.6$ nm, and g_1, g_2, τ_B as defined in Section II-B3. In addition, the pulse duration of the primary Stokes pulse and the conversion efficiency integrated over the full temporal profile are given.
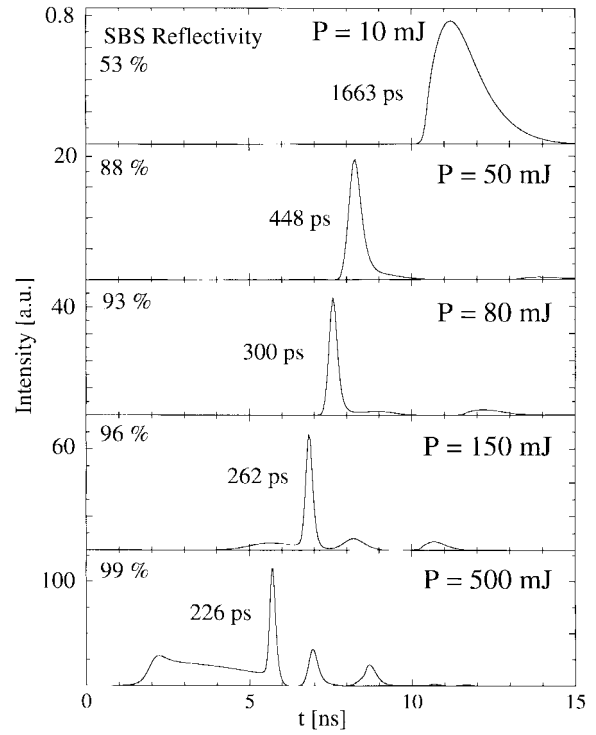

Fig. 4. Numerically generated temporal intensity profiles of SBS pulses emitted from the compact SBS generator-amplifier setup (methanol, $f = 10$ cm, $d_p = 6.5$ mm), plotted at various input energy levels P. In addition, the pulse duration of the primary Stokes pulse and the conversion efficiency integrated over the full temporal profile are given.

in complex pulse trains. At low pump energy, stimulated scattering initiated from spontaneously scattered Brillouin radiation only evolves from the focal region at the far end of the cell. At high pump energy, this region extends toward the cell input window and gives rise to a leading shoulder in the pulse, which finally causes a dramatic increase of its duration. Pulse compression in the case of such saturated amplification in the cell is not effective, because the Stokes pulse traversing the medium faces a divergent pump beam of decreasing energy density. All these effects prohibit the application of a single-cell SBS generator for high-energy pulse compression.

In the CGAS, an uncontrolled extension of the region of stimulated scattering initiated from spontaneously scattered Brillouin radiation is prevented by the separation of the medium into a focused (generator cell) and an unfocused part (amplifier cell). Fig. 4 depicts a simulation of the CGAS output. Methanol is chosen as the SBS medium to allow a direct comparison of the numerical results with experimental data presented in Section III. Similar to the single-cell situation starting from low input energy, both the reflectivity and compression factor increase with increasing input energy. At $P = 80$ mJ, a single peak of short duration is generated. At the sharply rising onset of the Stokes pulse, an almost complete conversion of pump into Stokes radiation takes place, resulting in a strong amplification of this early part of the pulse. At the tail of the Stokes pulse, SBS back-conversion clips the high-intensity part, leaving behind a smoothly decreasing shoulder. The back-converted pump radiation is responsible for secondary Stokes structures which become fairly pronounced at input energies >100 mJ.

To analyze the compression process, i.e., the temporal reshaping occurring in the amplifier in detail, it is useful to inspect the Stokes pulse shape at various positions along the amplifier cell at a fixed input energy, as shown in Fig. 5. The pulse emerges from the generator cell as a broad, doubly peaked structure ($Z = 1$ cm). On its passage through the amplifier cell, the leading structure experiences strong amplification and compression, resulting in the primary Stokes pulse emitted from the CGAS ($Z = 99$ cm). The trailing peak is not amplified because of gain depletion by the leading peak.

In the literature, there is still a discussion on the theoretical minimum duration of an SBS pulse generated by an SBS compressor. In early studies, a limit $\tau_s^{min} \geq 1/\omega_B$ was derived (see [3], [17]); later, estimates such as $\tau_s^{min} \approx 0.1\,\tau_B$ (see [10]) or the relation $\tau_s^{min} \propto \sqrt{\tau_B}$ (see [26], [11]) were preferred. Our numerical model is not suited to predict ultimate limits because the second-order time-derivatives $\partial^2/\partial t^2$ were omitted [3]. For practical reasons, we will define a *useful* minimum value τ_s^{min} corresponding to the duration of the primary Stokes pulse. At very high input energies (see lower panel of Fig. 4), peak structures of considerably shorter duration can be produced, but these are not useful since they are part of a multiple-peak structure. The phonon lifetime of methanol is given by $\tau_B = 374$ ps (Table I). An estimate for the useful minimum Stokes pulse duration of $\tau_s^{min} \approx 2/3\,\tau_B$ follows from present calculations for the CGAS.

The efficiency of the SBS conversion process becomes apparent by plotting the instantaneous pump pulse intensity
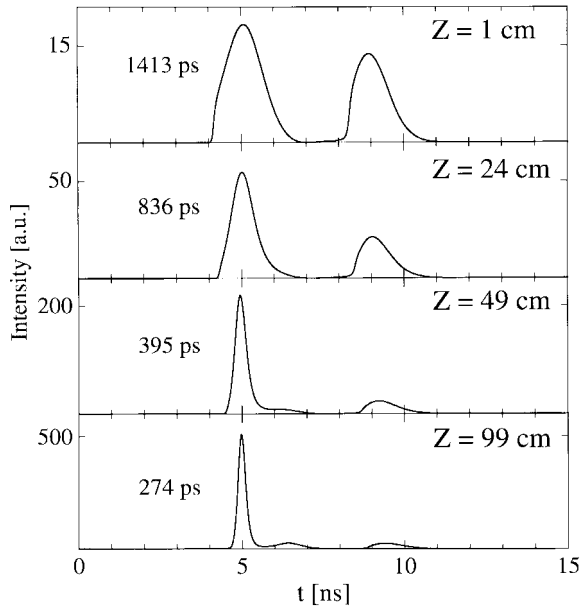
Fig. 5. Numerically generated temporal intensity profiles of SBS pulses emitted from the CGAS (methanol, input energy $P = 90$ mJ), calculated at various positions Z in the amplifier cell. The positions are defined as distances from the focusing lens (see Fig. 2). Hence at $Z = 1$ cm, the Stokes pulse is just emerged from the generator cell and enters the amplifier cell.

Fig. 6. Numerically generated intensity distribution of the pump pulse ($P = 90$ mJ) in the CGAS (methanol) dependent on position and time. The horizontal axis of the density plot represents the position in the compressor; time is evolving from the bottom to the top of the graph. High-intensity values of the pump intensity are represented in dark. The Stokes pulse evolution is easy to recognize also as a narrow zone of zero pump intensity counterpropagating with respect to the pump pulse at negative slope.

on a space-time grid of the modeled CGAS, as shown in Fig. 6. The intensity of the pump pulse immediately drops after contact with the Stokes pulse due to SBS conversion, leaving behind a zone of almost zero pump intensity. Directly behind this zone, a negligible fraction of pump intensity reappears, being generated by SBS back-conversion of Stokes into pump radiation. It is clear that no external beam attenuator in front of the generator cell is necessary for the CGAS to protect it against the pump peak intensity, as long as $L_a \geq \frac{1}{2} c \tau_p$.

Two effects limit the application of arbitrary high input energies in the CGAS: at a certain pump energy, the threshold for stimulated scattering initiated from spontaneously scattered Brillouin radiation is exceeded in the amplifier cell. It starts acting as an "SBS mirror" and becomes opaque. A clear sign of this activity is a broad structure preceding the primary Stokes pulse, as can be seen in Fig. 4 at $P = 500$ mJ. It is practical to define a *useful* reflectivity of the CGAS as well to discriminate against the "SBS mirror" regime of unity conversion efficiency. The useful reflectivity corresponds to the fraction of the input energy, which is back-scattered in the primary single Stokes pulse as part of the total complex emission structure. Referring to Fig. 4, the useful reflectivities at $P = 80$-, 150-, and 500-mJ input energy are 80%, 56%, and 23%, respectively. Surpassing the threshold for "SBS mirror" activity can be circumvented by choosing a larger pump beam diameter d_p in the amplifier cell to reduce the pump energy density. A severe limitation at high input energy is the effect of SBS back-conversion and thus the creation of secondary structures in the CGAS output. It results in a drop of the useful reflectivity as well. It depends on the application at which level the secondary structure intensities are no longer acceptable over the gain in compression factor.
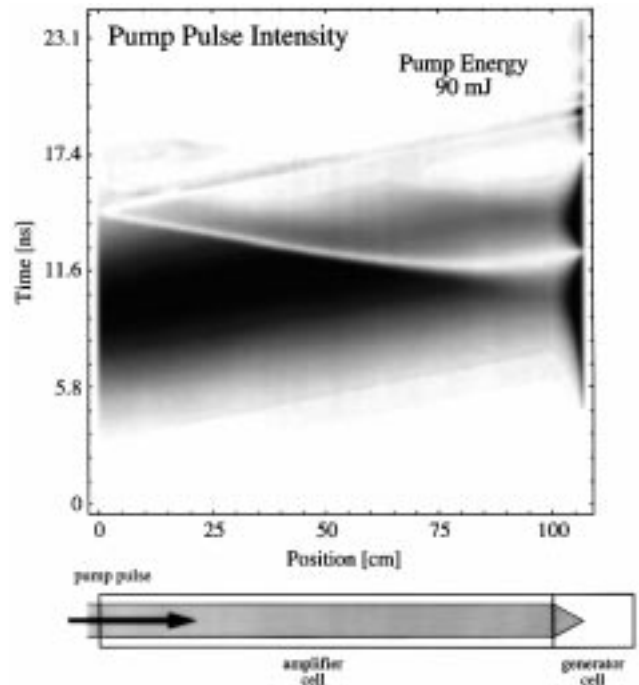
Related to the notion of a useful reflectivity and minimum pulse duration of a compressor is the specification of its intensity reflectivity. It is defined as the increase in peak intensity of the output pulse compared to the peak intensity of the input pulse. The occurrence of secondary structures in the output reduces the intensity reflectivity of a compressor. Referring to the results presented in Fig. 4, the CGAS is capable of producing an intensity reflectivity of larger 2000%.

III. THE COMPACT SBS GENERATOR-AMPLIFIER SETUP: EXPERIMENTS

All experiments were performed in glass cells of inner diameter 4 cm in the configuration depicted schematically in Fig. 2; the dimensional parameters are given in Section II-B3. The SBS-active liquids used were methanol, water, and tetrachloromethane (CCl_4), respectively, at room temperature. Liquid cyclohexane was investigated too, but it could not be reliably employed because of strong Raman activity. Solid contaminations in the SBS medium of the generator cell were minimized by filtering the liquid with membranes of 200-nm pore diameter. This procedure results in a substantial decrease of optical breakdown events in the focus region of the generator. The injection-seeded Nd:YAG laser source (Quanta-Ray GCR3) with a beam diameter of 6.5 mm had an output power up to 350 mJ in a single longitudinal mode at 532 nm at 10-Hz repetition rate and a pulse duration of 5.6 ns. Back-scattered Stokes radiation was separated from the incident laser light using a combination of a Fresnel-rhomb and a polarizing

beam splitter. It implies the propagation of circularly polarized light in the SBS cells. Beam-expansion optics were mounted in front of the amplifier cell to control the beam diameter d_p entering the CGAS. None of the optical elements including the entrance- and exit-windows of the cells as well as the beam separation optics were antireflection coated.

A. CGAS Compression Factor

Temporal profiles of the SBS pulses were recorded in two ways. In one method, we used a PIN photodiode of bandwidth 6 GHz and a digital oscilloscope of 1-GHz analogue bandwidth and a sampling rate of 5 GS/s. The temporal resolution of this system was checked by monitoring femtosecond pulses and reached 450-ps minimum pulse duration at FWHM. For high-resolution detection purposes, a streak camera of type Hadland Imacon 500 was applied.

1) Pump Energy Dependence: In Fig. 7, temporal Stokes pulse profiles emitted from a water-filled CGAS measured at various pump energies P are shown. Data were recorded either by integrating over the total spatial pump beam diameter [Fig. 7(a)] or from the central part only [Fig. 7(b)], using a 2.5-mm pinhole. Both series reveal a pump energy dependency as shown in Fig. 8. We find that the Stokes pulse duration τ_s reduces as the pump energy increases. Compared to the data taken at the beam axis, the integrated intensity profiles show nearly a factor of two larger pulse durations. This effect is ascribed to the reduced intensity in the wings of the spatial profile of the Nd:YAG beam as well as to a slight drop in the coherence properties of the beam at increasing off-axis distance. Consequently, the off-axis compression factor reduces as well. For a beam diameter $d_p = 9.75$ mm, the minimum useful pulse duration is approached at approximately 260-mJ input energy. Larger energies force the amplifier cell into the SBS mirror regime (cf. Section II-C). A bright diffuse spot overlapping the compact spatial Stokes beam profile at the exit of the beam separation optics is then observed. An appropriate way of pushing this regime toward higher input energies is the enlargement of the beam diameter d_p in the amplifier. Choosing, for instance, a beam diameter of 13 mm instead of 9.75 mm permits operation without diffuse SBS emission at a pump energy up to 300 mJ. The maximum compression factor is slightly reduced by this procedure, probably indicating spherical aberration of the focusing lens. The choice of a focusing lens with a focal length larger than 10 cm resulted in lower compression factors. A change to a smaller value caused frequent optical breakdown in the medium.

2) Minimum Stokes Pulse Duration: The data presented in Section III–A1 were recorded at 450-ps time resolution. Consequently, the minimum pulse durations of approximately 600 ps detected at 300-mJ input energy represent an upper limit to the actual pulse durations only. It necessitates higher time resolution to investigate minimum values for τ_s generated by the CGAS. This was achieved in streak camera measurements. The temporal resolution of the camera including subsequent image detection and digitizing was approximately 10 ps. Methanol was chosen as the SBS liquid because of its lower
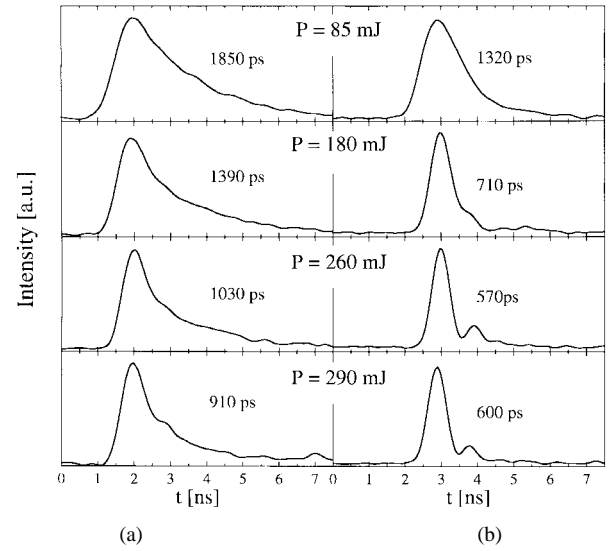

Fig. 7.   Temporally resolved Stokes output from the CGAS (water, $d_p = 9.75$ mm) at various pump energies P, detected with 450-ps time resolution. (a) Data recorded by integrating over the total spatial pump beam diameter. (b) Data recorded by integrating over the central part of the beam (diameter of 2.5 mm).
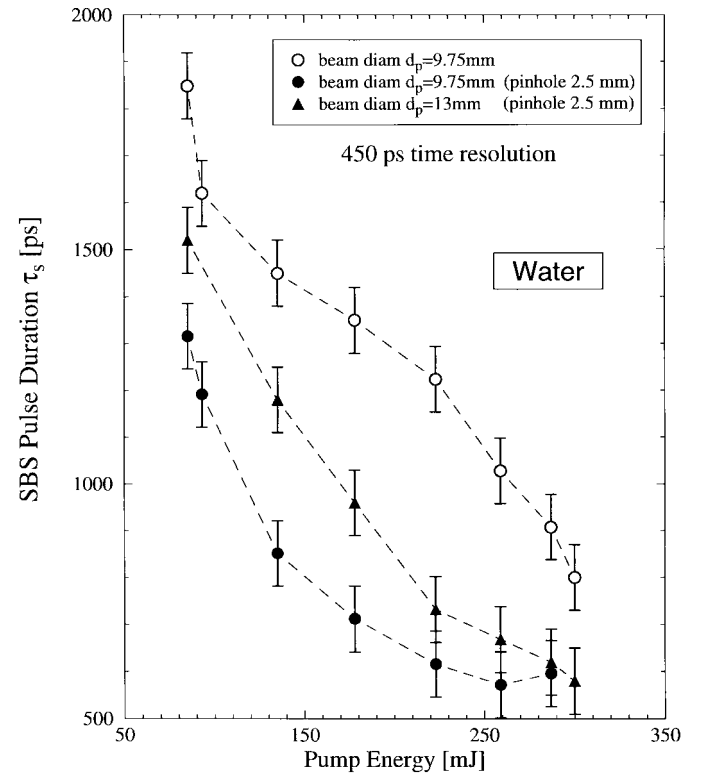

Fig. 8.   Measured duration of Stokes pulses emitted from the CGAS (water) plotted against the pump pulse input energy at different beam diameters, detected with 450-ps time resolution. Open circles represent measurements integrated over the total spatial pump beam diameter, filled circles the corresponding measurements on only the central part of the beam. Triangles represent results of a measurement at a larger beam diameter.

phonon lifetime compared to water (cf. Table I), which should lead to lower Stokes pulse durations.

In Fig. 9, a line of a streak record of the Stokes pulse emitted from the CGAS at 90-mJ input energy at a beam diameter of
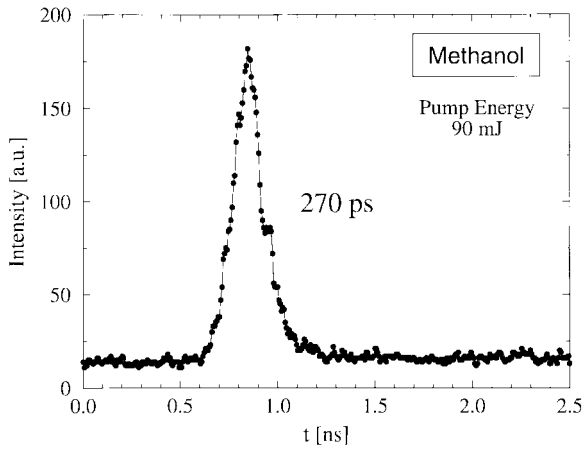
Fig. 9. Streak camera image at 10-ps resolution of SBS output from the CGAS (methanol, $d_p = 6.5$ mm) at 90-mJ pump energy. Only the central part of the beam (diameter of 2.5 mm) is exposed to the camera. Shown is one line of the 2-D image digitized at 8-b intensity resolution and at 6.5-ps time steps. Due to a nonlinear intensity response of the detection system, the half-maximum intensity level corresponds to 30% of the peak intensity, determined experimentally with the help of a 50% attenuator.
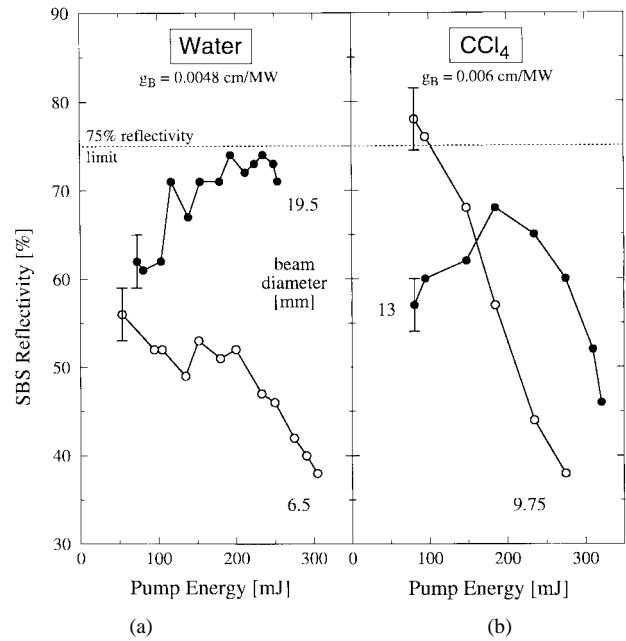

Fig. 10. Measured SBS reflectivity of the compact SBS generator-amplifier setup plotted against pump input energy for different beam diameters: (a) CGAS water-filled and (b) CGAS tetrachloromethane-filled. The 75% reflectivity level represents the maximum reflectivity of the CGAS, taking into account reflection losses due to uncoated optics. It corresponds to 100% internal SBS reflectivity.

6.5 mm is shown. Only radiation from the beam center was detected by using a pinhole of 2.5-mm diameter. The pulse has a rather symmetric shape and its pulse duration is 270 ps FWHM, which is equivalent to a compression factor of 21. This value agrees well with a duration of 274 ps at $P = 90$-mJ input energy predicted by the numerical model presented in section 2.3, see Fig. 4 at $Z = 99$ cm. Higher pump energies resulted in an increase of the detected pulse duration. From this it follows that the profile of Fig. 9 represents an SBS reflected pulse of minimum duration in methanol.

A comparison of the temporal Stokes pulse profiles detected by the photodiode system (Fig. 7) with the streak record data of Fig. 9 illustrates that the ringing structures in the tails of the pulses shown in Fig. 7 have to be attributed to the slow response characteristics of the detection system.

B. CGAS Conversion Efficiency

The measured SBS conversion efficiency of the CGAS is shown in Fig. 10 for various pump energies and beam diameters. These data are corrected for diffuse SBS radiation emerging from the amplifier cell by introducing a diaphragm of 6.5-mm aperture in front of the energy detector when entering the SBS mirror regime. The useful reflectivity drops with increasing pump energy, as shown in traces represented by open circles in Fig. 10. When the diameter d_p is readjusted, a high conversion efficiency at high input energy can be achieved (filled circles in Fig. 10). At low SBS gain and large beam expansion, high input energies are permitted while obtaining optimum conversion efficiency.

A determination of the maximum reflectivity of the CGAS has to take into account reflectivity losses of both pump and Stokes beams at uncoated glass-air interfaces. As a result, 25% of the internal SBS reflectivity is lost in our setup. Thus, typical external reflectivity values of the CGAS of 65% at maximum compression factor correspond to an internal SBS reflectivity exceeding 85%.
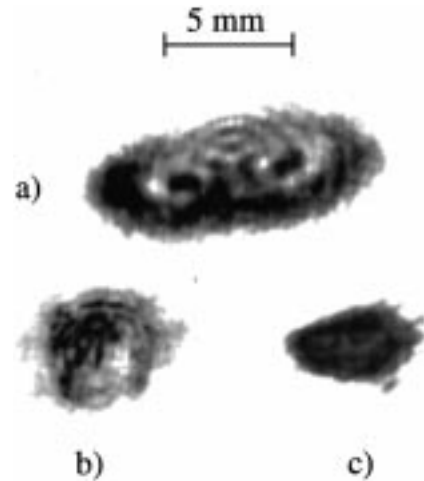

Fig. 11. Images of spatial beam profiles of (a) the pump beam at the exit of the CGAS, but with the compressor replaced by an ordinary mirror, (b) the CGAS output beam at its exit, and (c) the compressor output beam in the far-field at a distance of 7 m from the exit. The images were obtained by exposing photosensitive material to a single pulse of 100-mJ energy each.

C. CGAS Spatial Beam Profile

The spatial beam quality of the CGAS output is demonstrated in Fig. 11. These beam profile images were obtained by exposing photosensitive material to a single pulse of 100-mJ energy each. The gray-scale coding does not scale linearly with the intensity level; high intensity levels are overemphasized.

Fig. 11(a) depicts the spatial profile of the pump beam at the exit position of the CGAS, but with the compressor replaced by an ordinary mirror. Fig. 11(b) was produced by the Stokes beam detected at the same position as Fig. 11(a),

but emitted by the CGAS. Fig. 11(c) is a reproduction of the Stokes beam profile in the far-field at a distance of 7 m from the compressor exit. A comparison of these images shows that the compressor output is not diverging such as the pump beam of the Nd:YAG laser. Instead, it is much more homogeneous and slightly converging. This feature can be attributed to the phase-conjugation properties of the compressor.

It should be noted that the Nd:YAG laser source applied in this study is an older Quanta Ray version modified to produce a near Gaussian spatial beam profile and resembling the specifications of a Quanta-Ray GCR3 laser. From a modern Nd:YAG laser system with a better beam profile, an additional improvement in the compression and reflectivity properties of the CGAS may be expected.

IV. SUMMARY AND CONCLUSION

In the present study, a pulse compressor based on stimulated Brillouin scattering in liquids was experimentally and theoretically investigated, providing the temporal compression of Fourier-transform limited nanosecond pulses of several 100 mJ energy, combining both a high conversion efficiency and a high compression factor. The compact two-cell generator-amplifier arrangement does not require external attenuation of the generator cell input energy. Pulses from an injection-seeded, frequency-doubled Nd:YAG laser of 300-mJ energy were compressed by a factor variable between 6 and 21. The reflectivity at this compression approached 75%, limited by optical component losses. This value corresponds to an internal SBS conversion efficiency of nearly unity. Using appropriate coatings, an SBS reflectivity exceeding 90% can in principle be extracted.

A prescription of how to optimize the CGAS for a specific pump energy of up to 500 mJ to achieve both a maximum compression factor and reflectivity can be given now. The gain g_B of the SBS liquid must have a low value. For this reason, water is favored in this study. The pump beam diameter d_p has to be chosen small enough to operate the amplifier cell just below the threshold of becoming an SBS mirror. The general SBS threshold relation $g_B I_p L_a \geq 25$ [19] holds as an estimate of the power density necessary to approach this regime. The focal length of the focusing lens must be selected as small as possible, at the limit of optical breakdown in the focus.

Practical limits in applying the CGAS are determined by the spatial pump beam quality and its homogeneity: hot spots in the beam profile will boost local opacities in the amplifier cell at high-energy density. Regions of poor temporal coherence in the beam will lack efficient SBS conversion in the CGAS and will be responsible for a low-compression performance integrated over the profile. The choice of large beam diameters d_p in the case of very high input energy is limited by spherical aberrations of the focusing lens. Keeping d_p at a reasonable value but switching to a liquid with a lower SBS gain g_B is a good alternative.

Fourier-transform limited pulses of several hundreds of millijoules of energy and a variable duration of 300–3000 ps can be applied in various nonlinear optical and laser-spectroscopic investigations. The application of the presented CGAS is advantageous, because pulses of tailored duration are not easily produced by standard laser systems. On the other hand, injection-seeded Q-switched Nd:YAG laser systems of 5–10-ns pulse duration as the input source for the compressor are present in many laser laboratories. Our compact SBS generator-amplifier setup provides a tool to compress the energetic content of such laser output and correspondingly to increase their peak intensity by more than an order of magnitude. The compression of tunable laser output, for instance from single-mode pulsed dye laser sources, can be achieved with the CGAS as well. As a challenging application of such pulses, we are in the process of investigating the generation of high harmonics in gases to set up a table-top coherent and tunable soft X-ray laser system for spectroscopic applications.

REFERENCES

[1] R. Y. Chiao, C. H. Townes, and B. P. Stoicheff, "Stimulated Brillouin scattering and coherent generation of intense hypersonic waves," *Phys. Rev. Lett.*, vol. 21, pp. 592–595, 1964.

[2] R. L. Sutherland, *Handbook of Nonlinear Optics*, Optical Engineering. New York: Marcel Dekker, Inc., 1996, vol. 52, ch. 13 and references herein.

[3] D. T. Hon, "Pulse compression by stimulated Brillouin scattering," *Opt. Lett.*, vol. 5, pp. 516–518, 1980.

[4] Y. Nizienko, A. Mamin, and B. Brown, "300 ps ruby laser using stimulated Brillouin scattering pulse compression," *Rev. Sci. Instrum.*, vol. 65, pp. 2460–2463, 1994.

[5] C. B. Dane, W. A. Neuman, and L. A. Hackel, "High-energy SBS pulse compression," *IEEE J. Quantum Electron.*, vol. 30, pp. 1907–1915, 1994.

[6] A. A. Offenberger, D. C. Thompson, R. Fedosejevs, B. Harwood, J. Santiago, and H. R. Manjunath, "Experimental and modeling studies of a Brillouin amplifier," *IEEE J. Quantum Electron.*, vol. 29, pp. 207–216, 1993.

[7] M. A. Davydov, K. F. Shipilov, and T. A. Shmaonov, "Formation of highly compressed stimulated Brillouin scattering pulses in liquids," *Sov. J. Quantum Electron.*, vol. 16, pp. 1402–1403, 1986.

[8] C. B. Dane, L. E. Zapata, W. A. Neuman, M. A. Norton, and L. A. Hackel, "Design and operation of a 150 W near diffraction-limited laser amplifier with SBS wavefront correction," *IEEE J. Quantum Electron.*, vol. 31, pp. 148–162, 1995.

[9] M. J. Damzen and M. H. R. Hutchinson, "High-efficiency laser-pulse compression by stimulated Brillouin scattering," *Opt. Lett.*, vol. 8, pp. 313–315, 1983.

[10] V. A. Gorbunov, S. B. Papernyi, V. F. Petrov, and V. R. Startsev, "Time compression of pulses in the course of stimulated Brillouin scattering in gases," *Sov. J. Quantum Electron.*, vol. 13, pp. 900–905, 1983.

[11] R. Fedosejevs and A. A. Offenberger, "Subnanosecond pulses from a KrF laser pumped SF_6 Brillouin amplifier," *IEEE J. Quantum Electron.*, vol. QE-21, pp. 1558–1562, 1985.

[12] D. R. Hull, R. A. Lamb, and J. R. Digman, "Efficient phase conjugation at high energies using two cells," *Opt. Commun.*, vol. 72, pp. 104–108, 1989.

[13] G. J. Crofts and M. J. Damzen, "Steady-state analysis and design criteria of two-cell stimulated Brillouin scattering systems," *Opt. Commun.*, vol. 81, pp. 237–241, 1991.

[14] ———, "Experimental and theoretical investigation of two-cell stimulated-Brillouin-scattering systems," *J. Opt. Soc. Amer. B*, vol. 8, pp. 2282–2288, 1991.

[15] P. Narum, M. D. Skeldon, and R. W. Boyd, "Effect of laser mode structure on stimulated Brillouin scattering," *IEEE J. Quantum Electron.*, vol. QE-22, pp. 2161–2167, 1986.

[16] D. C. Jones, M. S. Mangir, D. A. Rockwell, and J. O. White, "Stimulated Brillouin scattering gain variation and transient effects in a CH_4:He binary gas mixture," *J. Opt. Soc. Amer. B*, vol. 7, pp. 2090–2096, 1990.

[17] M. J. Damzen and H. Hutchinson, "Laser pulse compression by stimulated Brillouin scattering in tapered waveguides," *IEEE J. Quantum Electron.*, vol. QE-19, pp. 7–14,1983.

[18] F. Dizier, J.-L. Ayral, J. Montel, and J.-P. Huignard, "A phase conjugate Nd:YAG laser with beam steering," *Int. J. Nonl. Opt. Phys.*, vol. 2, pp. 229–245, 1993.

[19] R. W. Boyd, *Nonlinear Optics.*   New York: Academic Press, 1992.
[20] W. Kaiser and M. Maier, "Stimulated Rayleigh, Brillouin, and Raman spectroscopy," in *Laser Handbook*, F. T. Arecchi and E. O. Schulz-Dubois, Eds.   Amsterdam, The Netherlands: North Holland, 1972, vol. 2, pp. 1077–1150.
[21] W. Jinsong, T. Weizhong, Z. Wen, "Stimulated Brillouin scattering initiated by thermally excited acoustic waves in absorption media," *Opt. Commun.*, vol. 123, pp. 574–576, 1996.
[22] A. I. Erokhin, V. I. Kovalev, and F. S. Faizullov, "Determination of the parameters of a nonlinear response of liquids in an acoustic resonance region by the method of nondegenerate four-wave interaction," *Sov. J. Quantum Electron.*, vol. 16, pp. 872–877, 1986.
[23] W. T. Grubbs and R. A. MacPhail, "Rotational-translational coupling and asymmetric line shapes in the high resolution stimulated Brillouin gain spectra of liquid carbon disulfide," *J. Chem. Phys.*, vol. 97, pp. 8906–8914, 1992.
[24] A. I. Erokhin, V. V. Oleinikov, and A. A. Putilin, "Spectral structure of stimulated Brillouin scattering," *JEPT Lett.*, vol. 61, pp. 887–893, 1995.
[25] R. C. Weast, M. J. Astle, Ed., *CRC Handbook of Chemistry and Physics.* Boca Raton, FL: CRC Press, 1983.
[26] M. A. Davydov and I. N. Koshevnikova, "Laser-pulse compression by stimulated Brillouin scattering in liquids," *Phys. Lett. A*, vol. 127, pp. 345–346, 1988.

Stephan Schiemann was born in Berlin, Germany, on June 21, 1964. He received the Diploma in physics and the Ph.D. degree from the University of Kaiserslautern, Germany, in 1989 and 1994, respectively.

Presently, he is working as a Postdoctoral Research Fellow at the Vrije Universiteit, Amsterdam, The Netherlands. His research interests include coherent light-matter interactions, nonlinear optical processes, and the generation of coherent soft X-ray radiation.

Wim Ubachs received the Drs. degree in solid-state physics and the Dr. degree in 1986 from the University of Nijmegen. His dissertation concerned high-resolution laser spectroscopic studies of diatomic hydrides.

As a Post-Doctoral Research Fellow, he worked at the Dalian Institute of Chemical Physics, China, and the Department of Chemistry at Stanford University, Stanford, CA. Since 1988, he has been a Lecturer of Physics at the Vrije Universiteit, Amsterdam, The Netherlands, where his activities are aimed at the generation and spectroscopic application of coherent and tunable extreme ultraviolet radiation.

Wim Hogervorst has been a Professor in Atomic and Laser Physics at the Vrije Univeriteit, Amsterdam, The Netherlands, since 1986. He is the founder of the interdisciplinary Laser Centre, which opened in 1992, and he is the leader of a research group whose main areas of interest include laser spectroscopy of atoms and molecules, nonlinear optical processes, laser cooling and trapping of atoms, and solid-state laser development.